Article

Early tetrapod neck mobility modelled using an extant analogue

https://doi.org/10.1038/s41586-026-11158-3

Received: 12 December 2025

Accepted: 11 September 2026

Published online: 14 October 2026

Open access

Check for updates

Dana E. Korneisel[1,6]✉, Cassandra M. Donatelli[2], Linfang Han[3], Thomas A. Stewart[4], Andrew L. Traynor[1], Benjamin K. A. Otoo[1], Marcos Martinez[3], Tetsuto Miyashita[3,5,7], Emily M. Standen[3,7] & Hillary C. Maddin[1,7]

Tetrapods arose from lobe-finned fishes with a notochord-dominated axial column[1–3]. During this transition, the skull became separated from the shoulder girdle[4–6], giving rise to a neck region. This head–shoulder separation has generated hypotheses suggesting that neck mobility increased during the origin of tetrapods, facilitating the ecological transition towards more terrestrial habitats[4,5,7–9]. However, incompletely co-ossified vertebral components[10] have posed a challenge to modelling the mobility of these early tetrapod necks. Here we used material tests on the similarly configured axial columns of sturgeon to predict the capacities of the tetrapod neck region for lateral flexion, extension and rotation across the tetrapod stem. Our model indicates that the soft tissue-dominated axial column was surprisingly rigid, despite lacking co-ossified vertebral components. We estimate that most stem tetrapods could move their heads less than 6° laterally and less than 3° dorsally but could not rotate them. Notably, mobility did not shift in conjunction with the head–shoulder separation that occurred between the origin of tristichopterids (represented by *Eusthenopteron*) and that of more crownward stem tetrapods. Therefore, mobility in the tetrapod neck did not serve as a functional driver of head–shoulder separation. Instead, forelimb-driven locomotion, implicated in early tetrapods[11–14], provides a better functional explanation for the head–shoulder separation.

Since the head and trunk first became anatomically distinct in the earliest vertebrates, the interface between these two body regions has undergone a series of evolutionary transformations[3,5,9,15]. These include a distinct vagal neural crest population[16–19], neck musculature (that is, cucullaris)[20–22], specialized anterior spinal nerves (the accessory and hypoglossal nerves)[23–25] and shoulder girdle[6,15,26,27]. During all these transformations, full head motion (as opposed to intracranial motion) was never independent of trunk motion[5,6,9,28,29]. However, the skull–trunk linkage underwent a marked change during the origin of tetrapods when the skull and shoulder girdle separated, giving rise to a distinct neck region unique to tetrapods[1,5,6]. Documented in key stem tetrapods such as *Acanthostega*[4,8] and *Tiktaalik*[9], this head–shoulder separation has given rise to the hypothesis that neck mobility increased markedly through an increase in flexion, extension or rotation across the new neck region during the origin of tetrapods as they began to inhabit more terrestrial habitats[4,7–9]. The predicted increase in neck mobility has not been functionally tested.

Stem tetrapods have an axial column dominated by the soft tissue notochord, which they retain throughout adulthood[1–3,30,31] (Fig. 1). The notochord is surrounded by distinct cartilaginous or bony arches that lack bone-to-bone joints[32,33] (Fig. 1b,c and Extended Data Fig. 1). This condition predates the evolution of the vertebral column characteristic of most adult crown tetrapods in which the notochord is mostly replaced by bony centra. In such an axial column, each vertebral centrum is generally fused to a neural arch, and the vertebrae articulate with one another through inter-central and zygapophyseal joints[10]. Stem tetrapods lack these stiffening features, despite their hypothesized functional advantage in supporting the axial column for survival in increasingly terrestrial habitats[4,7–9]. These anatomical differences mean that the axial columns of stem tetrapods are not a joint-based system like those of crown tetrapods, making the 'soft' axial columns of stem tetrapods challenging to model. No modern tetrapods have an anatomically or functionally comparable axial skeleton[10]. To generate constrained estimates of the functional capability of the stem tetrapod neck, we sought an alternative model using phylogenetically independent but anatomically comparable extant analogues for which material testing can be performed.

We identified the lake sturgeon (*Acipenser fulvescens*) as the best available model for the soft axial column of stem tetrapods. Sturgeon retain an intact notochord into adulthood[34,35] and have comparable body dimensions to stem tetrapods (Extended Data Figs. 1 and 5). The notochord-dominated axial column of sturgeon, a secondary adaptation in this lineage, has an anatomical configuration similar to that of stem tetrapods in terms of the overall proportions of vertebral arches to the notochordal canal in cross-section (Extended Data Figs. 1 and 2). The arches are joined by unmineralized connective tissues rather than

[1]Earth Sciences Department, Carleton University, Ottawa, Ontario, Canada. [2]School of Engineering and Technology, University of Washington, Tacoma, WA, USA. [3]Department of Biology, University of Ottawa, Ottawa, Ontario, Canada. [4]Department of Biology, The Pennsylvania State University, State College, PA, USA. [5]Canadian Museum of Nature, Ottawa, Ontario, Canada. [6]Present address: Department of Organismal Biology, Uppsala University, Uppsala, Sweden. [7]These authors jointly supervised this work: Tetsuto Miyashita, Emily M. Standen, Hillary C. Maddin. ✉e-mail: dana.korneisel@ebc.uu.se

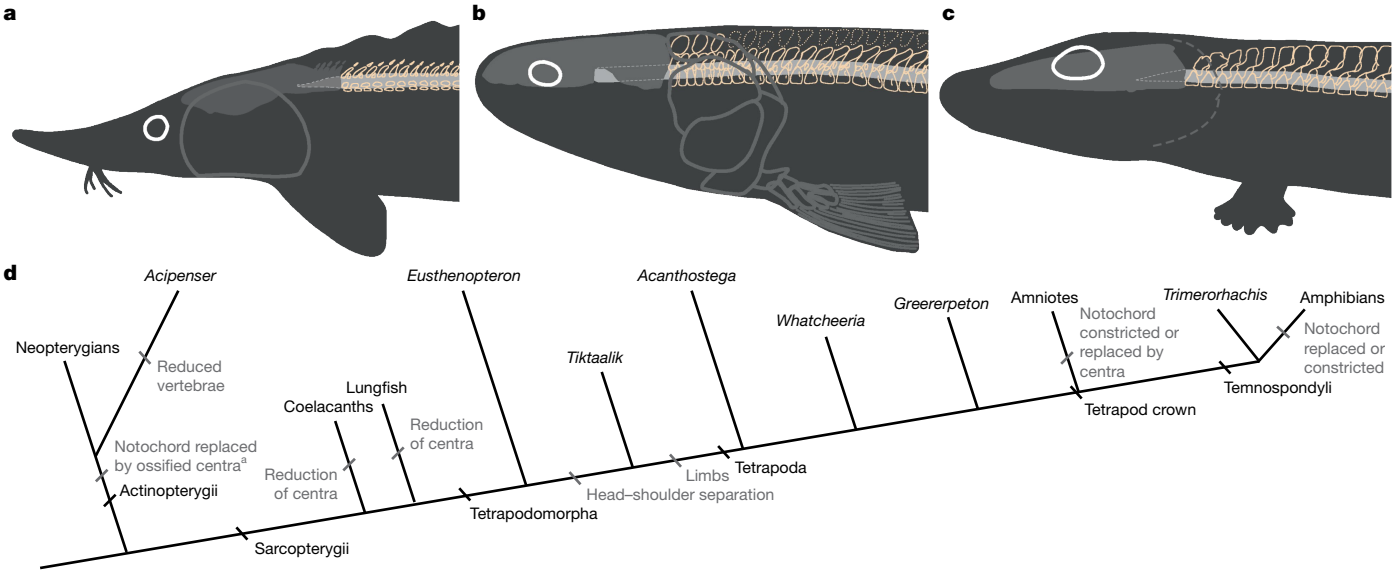


Fig. 1 | Evolution of the axial column during the origin of tetrapods. a, The anterior axial column of the lake sturgeon (*A. fulvescens*) showing the opercular bones; only the external operculum edge is outlined. Vertebral arches are shown in beige. Select skull elements are shown in dark grey, with opaque bone and translucent cartilage; the notochord is represented in pale grey and the white circle indicates the approximate position of the eye. **b**, The anterior axial column of *E. foordi* showing the ancestral tetrapodomorph condition, based on previously published studies[3,30]. Supraneurals posterior to the third supraneural are not illustrated but are presumed to be present anterior to the dorsal fin, as in other fishes. **c**, The anterior axial column of *A. gunnari* showing the limbed tetrapodomorph condition, based on previously published studies[2,63,64]. The dashed grey line indicates the posterior edge of the lateral skull. *Eusthenopteron* (**b**) and *Acanthostega* (**c**) are extinct. **d**, Phylogenetic relationships among the taxa examined in this study with clades denoted in black and relevant anatomical shifts in grey. [a]Several secondary losses of central ossification occur in actinopterygians.

by zygapophyseal joints[34,35] and the ventral vertebral components are multipartite (basidorsals and basiventrals in sturgeon; pleurocentra and intercentra in stem and early tetrapods)[34]. Some anatomical details of sturgeon vertebrae differ from those of their counterparts in stem and early tetrapods. Two examples are that sturgeon have supraneurals and that the basidorsals and basiventrals are placed dorsoventrally across the notochord from one another[34], whereas the intercentra and pleurocentra in stem and early tetrapods are staggered relative to one another but both ventrolateral to the notochord (Extended Data Fig. 2)[34]. Acknowleging these minor differences, we performed a series of material tests on the axial column and notochord of sturgeon specimens and measured lateral flexion stiffness, extension stiffness and torsional (rotational) stiffness. We then applied these stiffness values to the axial column dimensions of stem and early tetrapod taxa to determine the column rigidity and estimate neck mobility in these species.

The sturgeon axial column model

The mobility of a notochord-dominated axial column is limited by its material properties rather than by zygapophyseal articulations. This type of column is composed of soft tissue (notochord), hard tissue (cartilage or bony arches) and the connective tissues that unite them, all of which contribute to the material properties of the column. Notochord stiffness has been measured in hagfish[36], salmon embryos[37] and tadpoles[38], and its angular stiffness and internal pressure have been calculated in sturgeon during swimming[35] (Supplementary Table 3). In hagfish, notochord stiffness alone accounts for most of the body stiffness[36]. By contrast, reduced ossification of the anterior-most vertebrae in some dragonfish provides the notochordal column with much greater mobility than the rest of the column with ossified centra[39]; thus, the tissues surrounding the notochord may considerably increase the stiffness of the whole notochordal axial column in non-cyclostomes. To test their relative contributions to body stiffness, we measured the stiffness of both the isolated notochord and the whole column for our range-of-motion estimates of the early tetrapod axial column.

In sturgeon, the whole axial column approximates axial mobility better than does an isolated notochord. Our data indicate that notochord stiffness is not the limiting factor for axial column mobility in sturgeon, as the stiffness of the whole column (with intact mineralized arches and connective tissue) is considerably higher than that of the notochord alone (Table 1 and Supplementary Fig. 4). This high column stiffness is not attributable to hard stops or joint interactions between the arches, as we did not observe any such interactions or regionalization of bending during testing. Only negligibly small forces and torques were required to bend and twist the notochord compared with the whole column (Extended Data Table 1, Supplementary Table 4 and Supplementary Fig. 4). Therefore, we used whole-column stiffness to estimate the flexural rigidity of the similarly configured necks of stem tetrapods (Methods).

In lateral flexion, the sturgeon's posterior precloacal and tail regions of the axial column are less stiff than the anterior-most section (Extended Data Fig. 3 and Supplementary Table 5), located just posterior to the fused occipital vertebrae (these are unique to sturgeon in our dataset; Fig. 1). Stiffness was consistent along the column for the other measurements (Extended Data Figs. 3–5 and Supplementary Tables 6 and 7). To account for this variation for sturgeon, we used the Young's modulus from the anterior-most testing position for lateral flexion (Table 1), as this area is most comparable anatomically to the neck region in stem tetrapods.

Neck mobility is highly constrained

To estimate tetrapod neck mobility, we selected five stem tetrapods (*Eusthenopteron foordi*[3,30,31,40], *Tiktaalik roseae*[41], *Acanthostega gunnari*[2], *Whatcheeria deltae*[42] and *Greererpeton burkemorani*[43]) and one crown tetrapod (*Trimerorhachis insignis*[44–47]) for which axial column dimensions (Extended Data Fig. 1) are measurable. The vertebral components in these taxa are sufficiently preserved to enable the reconstruction of the anterior-most axial column and the estimation of the

Table 1 | Bending and torsional stiffness values

Measurement	*E* or *G* (GPa)
Lateral bending (*E*)	
Notochord only	0.45–0.52
Whole column	1.51–1.82
Dorsoventral bending (*E*)	
Notochord only	0.55–1.07
Whole column	0.95–1.35
Torsion (*G*)	
Notochord only	2.11×10^{-4}–2.44×10^{-4}
Whole column	2.1–3.95

Values were computed using materials tests on *A. fulvescens* ($n = 10$). *E*, Young's modulus or bending stiffness; *G*, torsional stiffness.

body cross-sectional area at the neck. On the basis of the material tests using sturgeon specimens, we estimated that neck mobility is constrained strongly by the axial column in these taxa.

Lateral flexion and extension

To estimate lateral flexion and extension (head elevation), we first determined the second moment of area for the anterior axial column (equation (3); Methods) and then calculated the force (F) required to achieve a given deflection (δ) (equation (8); Methods).

$$F = \frac{\delta 3EI}{L^3}$$

where E is Young's modulus (Pa) calculated from material tests of sturgeon specimens, I is the second moment of area (m^4) of the relevant section of the axial column and L is the length (m) of the cervical region or its equivalent. We next calculated the muscle cross-sectional area required to generate these forces, using the known pressures for striated muscles in vertebrates (Methods). These muscle areas were capped for each taxon at half the area of an oval fitted around the occiput to provide an absolute maximum muscle area available for lateral flexion (area on one side) and extension (combined dorsal area of both sides; Supplementary Fig. 3). The resulting estimates of the maximum range of motion represent the angles of deflection produced by the maximum force from the corresponding muscle area.

Our modelling revealed only modest neck mobility (Fig. 2) in the tetrapodomorphs *Eusthenopteron* (lateral flexion of 8.5°) and *Tiktaalik* (lateral flexion of 5.5°)—the earliest-diverging stem tetrapods in our dataset. Except for *Whatcheeria*, stem tetrapods were generally not capable of lateral neck flexion of more than 8.5° or neck extension of more than 3°. Among early tetrapods, *Acanthostega*, *Greererpeton* and *Trimerorachis* showed even lower estimates for lateral flexion (<3°) and extension (<1.5°) than their fish outgroups. We generated these estimates for the notochord-dominated anterior-most region of the axial column[30,41], where the column is much taller dorsally than it is wide in cross-section (Extended Data Fig. 2c). The column height was at least 166% of the column width in all tetrapods except *Tiktaalik* and *Greererpeton* (155% in *Tiktaalik*; only 128% in *Greererpeton*). In *Eusthenopteron*, this height was due to the presence of supraneurals[3] (not illustrated in Extended Data Fig. 2a), whereas in other stem and early tetrapods, it was due to the relatively tall neural arches (Extended Data Fig. 2c,d,f). No matter whether height comes from supraneurals or tall neural arches, our estimates generally suggest that taller axial columns have less mobility than do shorter ones.

In a notochord-dominated axial column, the length of the bending region also affects mobility, as the force required to achieve lateral flexion or extension decreases as a cubic function of length (see equation (8); Methods). This inverse cubic function partly explains the low

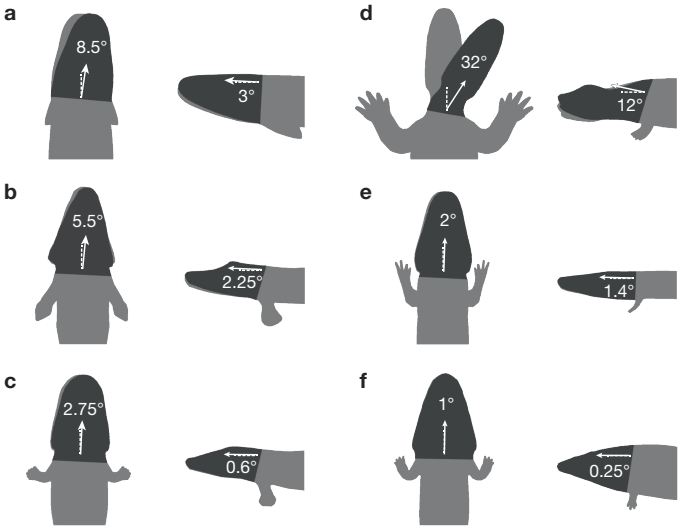


Fig. 2 | Estimates of lateral flexion and extension. a–**f**, Range-of-bending estimates in the neck (or analogous) region for *E. foordi* (**a**), *T. roseae* (**b**), *A. gunnari* (**c**), *W. deltae* (**d**), *G. burkemorani* (**e**) and *T. insignis* (**f**), as limited by axial column stiffness. Silhouettes are not drawn to scale relative to one another. Calculated estimates of lateral flexion and extension, along with neck length data, are provided in Extended Data Table 2.

estimates of neck mobility in *Acanthostega* and *Greererpeton* and the particularly short-necked *Trimerorhachis* (1° of lateral flexion and <1° of extension with only three neck vertebrae). Conversely, we attribute the surprisingly high estimated neck mobility in *Whatcheeria*, in part, to its long neck (Extended Data Fig. 2d). Our modelling suggests that *Whatcheeria* could achieve up to 32° of lateral flexion and 12° of extension, which exceed our estimates for other early tetrapods by approximately tenfold (lateral flexion) and eightfold (extension). It has a substantially longer neck (89% of the skull length) than other early tetrapods (34.2% of the skull length in *Acanthostega* and 37.6% in *Greererpeton*)[42]. Thus, *Whatcheeria* seems to be an outlier among early tetrapods in terms of both neck length and mobility; others generally had a highly limited range of head motion.

Rotation

To estimate the torques in the axial column required for head rotation, we used the modulus of rigidity (G) averaged from the material tests in sturgeon using equations (5)–(7) (Methods) and determined the polar moments of area (J) based on measurements obtained from the axial columns of stem and early tetrapods using equation (5) (Methods):

$$GJ = \frac{TL}{\theta}$$

where T is the maximum torque (Nm), L is the gauge length (m) and θ is the angle at maximum torque (degrees). We calculated torque (T) at small angles (5–10°) and found that the column required very high torques to achieve any rotation (≥200 Nm for 5°; Extended Data Table 1).

These high torque estimates suggest that large head turns are infeasible across the tetrapod stem, even in taxa with distinct atlas and axis vertebrae (notably, *Greererpeton* among the taxa examined here)[2,10,42,43,46]. We calculated the torques required to produce small 5° head turns in each taxon because the current knowledge of muscular anatomy is insufficient to estimate the maximum rotation achievable by the axial musculature (Extended Data Table 1). Among the taxa examined here, *Tiktaalik* required the lowest torque (200 Nm) for a 5° head rotation (Extended Data Table 1). This estimated torque is considerable given the limited length of the musculoskeletal elements that form the lever arm (for example, the cervical ribs). All other examined taxa, including *Eusthenopteron*, would require even higher torque (314–746 Nm) than

that required in *Tiktaalik* for the same degree of rotation (Extended Data Table 1).

Discussion

Factors influencing axial column bending

Variations in the maximum lateral flexion and extension estimates for stem and early tetrapods are correlated with differences in the body proportions, especially the neck length, of the species analysed. The estimated maximum lateral flexion values of *Trimerorhachis*, the taxon with the shortest neck (<3 cm, 19% of its skull length; Supplementary Table 5), and *Whatcheeria*, the taxon with the longest neck (nearly 20 cm, 89% of its skull length; Supplementary Table 5), differ by 31°. However, the overall neck length and the number of vertebrae in the neck region are similar across most stem tetrapods (*Eusthenopteron*, *Tiktaalik*, *Acanthostega* and *Greererpeton*). Although *Eusthenopteron* lacks a distinct cervical region defined by the area between the skull and shoulder girdle, an equivalent region can still be identified in the anterior-most axial column by anatomically distinguishable vertebrae (that is, ribless centra or broad supraneurals, depending on the specimen)[3,30,40]. We measured the axial column length in this region to model theoretical mobility if the region were free (Extended Data Table 2 and Extended Data Fig. 2). The lateral flexion capacities of the axial columns of *Eusthenopteron* and *Tiktaalik* exceed those of *Acanthostega* and *Greererpeton* by two- to threefold (Fig. 2 and Extended Data Table 2), despite comparable neck lengths. These differences seem to result from variations in the geometries of both the axial column and body cross-sections (Extended Data Fig. 2 and Supplementary Fig. 3).

Axial column geometry influences the moment of inertia (*I* in equations (8) and (9); Methods), whereas the body cross-sectional area limits the maximum muscle area (Methods and Supplementary Fig. 3). The ratio of vertebral width to height affects *I* and, therefore, the column mobility, especially in extension. In *Tiktaalik*, the vertebrae are nearly as tall as they are wide at the base and this enables 2.25° of extension (Extended Data Figs. 1c,e and 2b; similar to *Greererpeton*, Extended Data Fig. 2e). Vertebral height is greater in other taxa (up to 2.17 times the width in *Acanthostega*; Extended Data Table 1 and Extended Data Fig. 2c) and extension is correspondingly lower (0.6° in *Acanthostega*; Fig. 2 and Extended Data Table 2). To further assess how vertebral proportions affect bending, we calculated bending for a theoretical 10 cm-long neck with the column of each taxon scaled to the same width. We found not only that tall and narrow vertebral proportions are indeed restrictive, especially in *Acanthostega*, but also that the rectangular profile of *Trimerorhachis* strongly restricts bending even in a long axial column section, so its low head mobility is only partly due to its very short neck (Supplementary Table 9).

Crownward tetrapods tend to have a relatively wide axial column, as seen in *Greererpeton* (Extended Data Fig. 2e). This is due in part to robust transverse processes[33]—a geometry that is favourable for greater mobility (Supplementary Table 9). In other taxa, such as embolomeres and amniotes, this widening is also correlated with an increasing replacement of the notochord by vertebral centra. Our current method is inappropriate for estimating the range of mobility in taxa such as these, with restricted notochords. The zygapophyseal connections between vertebrae are also elaborated in crown tetrapods, adding complex joints to the vertebral column. Evaluating early tetrapod and early amniote axial columns with more developed zygapophyseal articulations will require a different approach.

Further constraints on neck mobility

Our estimates of lateral flexion, extension and rotational capacities are based on the flexural and torsional rigidity of the axial column. In a whole body, additional tissues superficial to the axial column—namely the integument, muscles, osteoderms and ribs—also contribute considerable stiffness[48]. Further constraints on tetrapod neck mobility could also arise from internal organs that cannot tolerate the extension or compression caused by head motion, such as the gill apparatus in, for example, *Eusthenopteron*[40], *Tiktaalik*[49] and *Acanthostega*[50].

The axial column and terrestrialization

Our models of neck mobility across stem and early tetrapods contradict the predicted increase in neck mobility driven by head–shoulder separation[4,7–9]. Instead, they suggests that the separation event (which occurred among the common ancestors shared by *Tiktaalik* and *Acanthostega* but was not shared with *Eusthenopteron*[9,49]) had no detectable effect on neck mobility (Fig. 2). Overall, stem tetrapods had stiffer necks than might be expected given their soft tissue-dominated axial columns (the properties assessed are summarized in Supplementary Table 3). In these taxa, the capacities for lateral flexion and extension were limited to only a few degrees. Furthermore, the capacity for head rotation was absent or, at best, extremely limited in stem and early tetrapods. In exceptional cases among stem tetrapods (such as *Whatcheeria*) and derived crown tetrapods, the neck enables substantial and independent head motion; however, this ability seems to have evolved secondarily to the origin of the tetrapod neck (that is, head–shoulder separation).

Our results offer an alternative to the prevailing interpretation[4,5,7–9,51] that the separation of the skull and pectoral girdle indicates independent neck mobility through a free neck in stem tetrapods. A stiff axial column, as inferred from our analysis, is consistent with the amphibious lifestyle hypothesized for most stem tetrapods[4,7,8,51], in which low neck mobility may have been advantageous for locomotion in water by increasing energetic efficiency during swimming[52]. A stiff axial column may also have contributed to passive resistance to gravity in terrestrial environments. Thus, given the limited neck mobility in stem tetrapods, alternative functional explanations for the head–shoulder separation are warranted.

We argue that the head–shoulder separation is more consistent with the predicted origin of forelimb-driven locomotion in early tetrapods[4,11–14]. The pectoral fin and girdle underwent several anatomical changes across the tetrapod stem[8,12], including the rearrangement of the long bones and the loss of lepidotrichia[13,52–54]. *Eusthenopteron*, the earliest-branching tetrapodomorph considered, already has a stress-dissipating trabecular architecture in its humerus that could support weight bearing[14]. More derived stem tetrapods such as *Ichthyostega* are hypothesized to have used pectoral-powered locomotion in contact with the substrate[11,42,51,55,56], similar to the terrestrial locomotion observed in several extant fishes[13,57,58]. These lines of inference reveal a trend of increasing demand on the shoulder girdle to support forelimb function[4,9,11,27,58] rather than to connect the head with the trunk[5,6,15] across the tetrapod stem. Thus, the head–shoulder separation in stem tetrapods probably resulted from this shift in primary shoulder function.

In fact, the tetrapod neck seems to have evolved as a by-product of the head–shoulder separation, rather than as an adaptation to increase neck mobility. Although the axial column remained generally stiff in stem tetrapods, derived tetrapods acquired greater neck mobility, partly by having longer necks and partly through the evolution of mobile intervertebral joints[59] that enable lateral flexion, extension[60] and rotation[61]. The delayed acquisition of neck mobility calls into question the relevance of some hypothesized terrestrial feeding modes for early tetrapods[51], because such limited head mobility would preclude lateral snapping when the forelimb was planted except, perhaps, in *Whatcheeria*[42]. Meanwhile, our results align with hypotheses regarding aquatic feeding behaviour that suggest that additional lateral flexion in the trunk contributes to overall motion[51,62] and broadly support amphibious locomotory habits among stem and early tetrapods[11,42,51,56].

Online content

Any methods, additional references, Nature Portfolio reporting summaries, source data, extended data, supplementary information,

acknowledgements, peer review information; details of author contributions and competing interests; and statements of data and code availability are available at https://doi.org/10.1038/s41586-026-11158-3.

1. Arratia, G., Schultze, H.-P. & Casciotta, J. Vertebral column and associated elements in dipnoans and comparison with other fishes: development and homology. *J. Morphol.* **250**, 101–172 (2001).
2. Coates, M. The Devonian tetrapod *Acanthostega gunnari* Jarvik: postcranial anatomy, basal tetrapod interrelationships and patterns of skeletal evolution. *Trans. R. Soc. Edinb.* **87**, 363–421 (1996).
3. Hitchcock, E. C. A functional interpretation of the anterior-most vertebrae and skull of *Eusthenopteron*. *Bull. Mus. Natl Hist. Nat.* **4**, 269–285 (1995).
4. Long, J. A. & Gordon, M. S. The greatest step in vertebrate history: a paleobiological review of the fish-tetrapod transition. *Physiol. Biochem. Zool.* **77**, 700–719 (2004).
5. Ericsson, R., Knight, R. & Johanson, Z. Evolution and development of the vertebrate neck. *J. Anat.* **222**, 67–78 (2013).
6. Hirasawa, T. & Kuratani, S. Evolution of the vertebrate skeleton: morphology, embryology, and development. *Zool. Lett.* **1**, 2 (2015).
7. Coates, M. I., Ruta, M. & Friedman, M. Ever since Owen: changing perspectives on the early evolution of tetrapods. *Annu. Rev. Ecol. Evol. Syst.* **39**, 571–592 (2008).
8. Clack, J. A. *Gaining Ground: The Origin and Evolution of Tetrapods* (Indiana Univ. Press, 2012).
9. Shubin, N., Daeschler, E. B. & Jenkins, F. A. Jr. Origin of the tetrapod neck and shoulder. In *Great Transformations in Vertebrate Evolution* (eds Dial, K. P. et al.) 63–76 (Univ. Chicago Press, 2015).
10. Korneisel, D. E. & Maddin, H. C. Review of the tetrapod skull–neck boundary: implications for the evolution of the atlas–axis complex. *Biol. Rev.* **100**, 2435–2470 (2025).
11. Pierce, S. E., Clack, J. A. & Hutchinson, J. R. Three-dimensional limb joint mobility in the early tetrapod *Ichthyostega*. *Nature* **486**, 523–526 (2012).
12. Coates, M. I. & Ruta, M. Skeletal changes in the transition from fins to limbs. In *Fins into Limbs: Evolution, Development, and Transformation* (ed. Hall, B. K.) 15–38 (Univ. Chicago Press, 2007).
13. Standen, E. M., Du, T. Y. & Larsson, H. C. E. Developmental plasticity and the origin of tetrapods. *Nature* **513**, 54–58 (2014).
14. Clarac, F., Cornille, A., Bijl, S. & Sanchez, S. Tetrapod terrestrialisation: a weight-bearing potential already present in the humerus of the stem-tetrapod fish *Eusthenopteron foordi*. Preprint at *bioRxiv* https://doi.org/10.1101/2024.02.09.579723 (2024).
15. Miyashita, T. et al. Novel assembly of a head–trunk interface in the sister group of jawed vertebrates. *Nature* **645**, 686–691 (2025).
16. Kuratani, S. Spatial distribution of postotic crest cells defines the head/trunk interface of the vertebrate body: embryological interpretation of peripheral nerve morphology and evolution of the vertebrate head. *Anat. Embryol.* **195**, 1–13 (1996).
17. Kuo, B. R. & Erickson, C. A. Vagal neural crest cell migratory behavior: a transition between the cranial and trunk crest. *Dev. Dyn.* **240**, 2084–2100 (2011).
18. Kuratani, S., Kusakabe, R. & Hirasawa, T. The neural crest and evolution of the head/trunk interface in vertebrates. *Dev. Biol.* **444**, S60–S66 (2018).
19. Martik, M. L. et al. Evolution of the new head by gradual acquisition of neural crest regulatory circuits. *Nature* **574**, 675–678 (2019).
20. Lescroart, F. et al. Clonal analysis reveals a common origin between nonsomite-derived neck muscles and heart myocardium. *Proc. Natl Acad. Sci. USA* **112**, 1446–1451 (2015).
21. Adachi, N., Bilio, M., Baldini, A. & Kelly, R. G. Cardiopharyngeal mesoderm origins of musculoskeletal and connective tissues in the mammalian pharynx. *Development* **147**, dev185256 (2020).
22. Swedlund, B. & Lescroart, F. Cardiopharyngeal progenitor specification: multiple roads to the heart and head muscles. *Cold Spring Harb. Perspect. Biol.* **12**, a036731 (2020).
23. Lours-Calet, C. et al. Evolutionarily conserved morphogenetic movements at the vertebrate head–trunk interface coordinate the transport and assembly of hypopharyngeal structures. *Dev. Biol.* **390**, 231–246 (2014).
24. Oisi, Y., Fujimoto, S., Ota, K. G. & Kuratani, S. On the peculiar morphology and development of the hypoglossal, glossopharyngeal and vagus nerves and hypobranchial muscles in the hagfish. *Zool. Lett.* **1**, 6 (2015).
25. Tada, M. N. & Kuratani, S. Evolutionary and developmental understanding of the spinal accessory nerve. *Zool. Lett.* **1**, 4 (2015).
26. Matsuoka, T. et al. Neural crest origins of the neck and shoulder. *Nature* **436**, 347–355 (2005).
27. Shubin, N. H., Daeschler, E. B. & Jenkins, F. A. Jr. The pectoral fin of *Tiktaalik roseae* and the origin of the tetrapod limb. *Nature* **440**, 764–771 (2006).
28. Camp, A. L. A neck-like vertebral motion in fish. *Proc. R. Soc. B* **288**, 20211091 (2021).
29. Jones, M. E. H. et al. The biomechanical role of the chondrocranium and the material properties of cartilage. *Vertebr. Zool.* **70**, 699–715 (2020).
30. Andrews, S. M. & Westoll, T. S. IX.—The postcranial skeleton of *Eustenopteron foordi* Whiteaves. *Trans. R. Soc. Edinb.* **68**, 207–329 (1970).
31. Andrews, S. M. & Westoll, T. S. XII.—The Postcranial skeleton of rhipidistian fishes excluding *Eusthenopteron*. *Trans. R. Soc. Edinb.* **68**, 391–489 (1970).
32. Ahlberg, P. E., Clack, J. A. & Blom, H. The axial skeleton of the Devonian tetrapod *Ichthyostega*. *Nature* **437**, 137–140 (2005).
33. Sumida, S. S. & Lombard, R. E. The atlas-axis complex in the late Paleozoic genus *Diadectes* and the characteristics of the atlas-axis complex across the amphibian to amniote transition. *J. Paleontol.* **65**, 973–983 (1991).
34. Leprévost, A., Azaïs, T., Trichet, M. & Sire, J.-Y. Vertebral development and ossification in the Siberian sturgeon (*Acipenser baerii*), with new insights on bone histology and ultrastructure of vertebral elements and scutes. *Anat. Rec.* **300**, 437–449 (2017).
35. Long, J. H. Jr. Morphology, mechanics, and locomotion: the relation between the notochord and swimming motions in sturgeon. *Environ. Biol. Fish.* **44**, 199–211 (1995).
36. Long, J. H. Jr, Koob-Emunds, M., Sinwell, B. & Koob, T. J. The notochord of hagfish *Myxine glutinosa*: visco-elastic properties and mechanical functions during steady swimming. *J. Exp. Biol.* **205**, 3819–3831 (2002).
37. Kryvi, H. et al. The notochord in Atlantic salmon (*Salmo salar* L.) undergoes profound morphological and mechanical changes during development. *J. Anat.* **231**, 639–654 (2017).
38. Adams, D. S., Keller, R. & Koehl, M. A. R. The mechanics of notochord elongation, straightening and stiffening in the embryo of *Xenopus laevis*. *Development* **110**, 115–130 (1990).
39. Schnell, N. K., Britz, R. & Johnson, G. D. New insights into the complex structure and ontogeny of the occipito-vertebral gap in barbeled dragonfishes (Stomiidae, Teleostei). *J. Morphol.* **271**, 1006–1022 (2010).
40. Jarvik, E. Structure of a Devonian fish: *Eusthenopteron foordi*. In *Basic Structure and Function of Vertebrates* Vol. 1, 99–194 (Academic Press, 1980).
41. Stewart, T. A. et al. The axial skeleton of *Tiktaalik roseae*. *Proc. Natl Acad. Sci. USA* **121**, e2316106121 (2024).
42. Otoo, B. K. A., Bolt, J. R., Lombard, R. E., Angielczyk, K. D. & Coates, M. I. The postcranial anatomy of *Whatcheeria deltae* and its implications for the family Whatcheeriidae. *Zool. J. Linn. Soc.* **193**, 700–745 (2021).
43. Godfrey, S. J. The postcranial skeletal anatomy of the carboniferous tetrapod *Greererpeton burkemorani* Romer, 1969. *Phil. Trans. R. Soc. B* **323**, 75–133 (1989).
44. Case, E. C. *A Revision of the Amphibia and Pisces of the Permian of North America* (Carnegie Institution of Washington, 1911).
45. Case, E. C. *Description of a Collection of Associated Skeletons of Trimerorhachis* (Univ. Michigan Press, 1935).
46. Shishkin, M. A. Evolution of the cervical vertebrae in temnospondyl amphibians and differentiation of the early tetrapods. *Paleontol. J.* **34**, 534–546 (2000).
47. Pawley, K. The postcranial skeleton of *Trimerorhachis insignis* Cope, 1878 (Temnospondyli: Trimerorhachidae): a plesiomorphic temnospondyl from the Lower Permian of North America. *J. Paleontol.* **81**, 873–894 (2007).
48. Molnar, J. L., Pierce, S. E., Bhullar, B.-A. S., Turner, A. H. & Hutchinson, J. R. Morphological and functional changes in the vertebral column with increasing aquatic adaptation in crocodylomorphs. *R. Soc. Open Sci.* **2**, 150439 (2015).
49. Daeschler, E. B., Shubin, N. H. & Jenkins, F. A. Jr. A Devonian tetrapod-like fish and the evolution of the tetrapod body plan. *Nature* **440**, 757–763 (2006).
50. Coates, M. I. & Clack, J. A. Fish-like gills and breathing in the earliest known tetrapod. *Nature* **352**, 234–236 (1991).
51. Hohn-Schulte, B., Preuschoft, H., Witzel, U. & Distler-Hoffmann, C. Biomechanics and functional preconditions for terrestrial lifestyle in basal tetrapods, with special consideration of *Tiktaalik roseae*. *Hist. Biol.* **25**, 167–181 (2013).
52. VanBuren, C. S. & Evans, D. C. Evolution and function of anterior cervical vertebral fusion in tetrapods. *Biol. Rev.* **92**, 608–626 (2017).
53. Boisvert, C. A., Mark-Kurik, E. & Ahlberg, P. E. The pectoral fin of *Panderichthys* and the origin of digits. *Nature* **456**, 636–638 (2008).
54. Stewart, T. A. et al. Fin ray patterns at the fin-to-limb transition. *Proc. Natl Acad. Sci. USA* **117**, 1612–1620 (2020).
55. Strong, C. R. C., Bishop, P. J., Hutchinson, J. R. & Pierce, S. E. Digital volumetric modeling reveals unique body plan experimentation in the Devonian tetrapod *Ichthyostega*. *iScience* **28**, 112486 (2025).
56. Molnar, J. L., Hutchinson, J. R., Diogo, R., Clack, J. A. & Pierce, S. E. Evolution of forelimb musculoskeletal function across the fish-to-tetrapod transition. *Sci. Adv.* **7**, eabd7457 (2021).
57. King, H. M., Shubin, N. H., Coates, M. I. & Hale, M. E. Behavioral evidence for the evolution of walking and bounding before terrestriality in sarcopterygian fishes. *Proc. Natl Acad. Sci. USA* **108**, 21146–21151 (2011).
58. Pierce, S. E., Hutchinson, J. R. & Clack, J. A. Historical perspectives on the evolution of tetrapodomorph movement. *Integr. Comp. Biol.* **53**, 209–223 (2013).
59. Jones, K. E., Brocklehurst, R. J. & Pierce, S. E. AutoBend: an automated approach for estimating intervertebral joint function from bone-only digital models. *Integr. Org. Biol.* **3**, obab026 (2021).
60. Werneburg, I. et al. Modeling neck mobility in fossil turtles. *J. Exp. Zool.* **324**, 230–243 (2015).
61. Krings, M., Nyakatura, J. A., Boumans, M. L. L. M., Fischer, M. S. & Wagner, H. Barn owls maximize head rotations by a combination of yawing and rolling in functionally diverse regions of the neck. *J. Anat.* **231**, 12–22 (2017).
62. Lemberg, J. B., Daeschler, E. B. & Shubin, N. H. The feeding system of *Tiktaalik roseae*: an intermediate between suction feeding and biting. *Proc. Natl Acad. Sci. USA* **118**, e2016421118 (2021).
63. Clack, J. A. The neurocranium of *Acanthostega gunnari* Jarvik and the evolution of the otic region in tetrapods. *Zool. J. Linn. Soc.* **122**, 61–97 (1998).
64. Porro, L. B., Rayfield, E. J. & Clack, J. A. Descriptive anatomy and three-dimensional reconstruction of the skull of the early tetrapod *Acanthostega gunnari* Jarvik, 1952. *PLoS ONE* **10**, e0118882 (2015).

Publisher's note Springer Nature remains neutral with regard to jurisdictional claims in published maps and institutional affiliations.

Open Access This article is licensed under a Creative Commons Attribution 4.0 International License, which permits use, sharing, adaptation, distribution and reproduction in any medium or format, as long as you give appropriate credit to the original author(s) and the source, provide a link to the Creative Commons licence, and indicate if changes were made. The images or other third party material in this article are included in the article's Creative Commons licence, unless indicated otherwise in a credit line to the material. If material is not included in the article's Creative Commons licence and your intended use is not permitted by statutory regulation or exceeds the permitted use, you will need to obtain permission directly from the copyright holder. To view a copy of this licence, visit http://creativecommons.org/licenses/by/4.0/.

© The Author(s) 2026

Methods

Materials

Ten *A. fulvescens* yearlings were partially dissected for material characterization. This number was not predetermined statistically. The fish were housed and cared for prior to being provided to us dead in accordance with the animal use protocol (22003) approved by the Canadian Council on Animal Care and Wilfrid Laurier University's Animal Care Committee. Additional specimens from the same source, as well as waste from commercially fished sturgeon, were used for test design and figures (Extended Data Table 3).

Material testing

The tested specimens were thawed and their axial columns were dissected out in the morning on the day of testing (Extended Data Fig. 1a, Supplementary Methods, Supplementary Table 1 and Supplementary Figs. 1 and 2). Each dissected axial column included a cube of bone and cartilage from the posterior-most section of the skull and the caudal fin to avoid cutting the notochord at any point along its length and compromising its mechanical properties. Dissected specimens were kept moist and stored on ice between dissection and testing and between trials. The column was dissected further on site for torsion testing of specific sections and for testing the notochord (Supplementary Methods). Tissue bending was measured on a ZwickiLine Z5.0 TN materials testing machine (ZwickRoell) using a ZwickRoell GTM series K load cell (5 kN capacity, International Organization for Standardization (ISO) 7500-1 accuracy class 1 from 20 N to 5 kN). Measurement electronics provide a 24 bit resolution across the range corresponding to a force resolution finer than 0.01 N; although our maximum loads fell below the threshold of the ISO, they remained well within the electronic resolution of the system and were repeatable across measurements. Torque was measured using a 20 Nm torque transducer (ISO 7500-1 accuracy class 1 from 0.2 Nm to 20 Nm) on the same machine. The full-scale range corresponds to a resolution finer than 0.0001 Nm; although some of our measured torques fell below the ISO threshold, they also remained well within the electronic resolution of the system. The first round of manipulation in each trial is the source of data in this study, with additional rounds being performed in case these data are of interest for future materials assessments.

Whole-column bending. First, three-point lateral bending (equivalent to lateral flexion) was performed with the supporting pins set at a 4 cm span and the loading pin set to a 5 mm depression depth (five rounds of depression per trial). Next, dorsoventral bending (equivalent to extension) was conducted with the same span but with the depression depth decreased to 3 mm to avoid bending the tissue to a damaging degree.

Whole-column torsion. After the bending tests, the column was dissected further into sections between every 12th rib and the subsequent rib. The skull cube was not removed to avoid cutting the anterior end of the notochord. Each section was clamped vertically in the machine with the anterior part facing upwards. The torsion drive was then rotated 30° clockwise, held for 1 s and returned to the starting position three times per trial.

Notochord bending. The notochord was dissected from each column. Lateral bending and dorsoventral bending were performed consequently with the supporting pins set at a 2 cm span and the loading pin set to a 3 mm depression depth (five rounds per trial). Small pieces of coarse sandpaper (60–100 grit) were placed between the sample and support points to stabilize the specimen when it rolled out of the desired orientation during set-up. We ensured that the added sandpaper did not overlap with the span between the supporting pins so as to avoid increasing the stiffness of the notochord area that was being tested.

Notochord torsion. Testing trials for specimens 2401-01 and 2401-02 followed the same protocol as for whole-column torsion measurements. During initial trials, we observed a sinusoidal curve indicative of viscoelastic properties. We therefore increased the hold time to 3 s at 30° for specimens 2401-04–2401-10.

Measurements

Sturgeon. Total column length (from skull cube to tail tip), torsion gauge length and notochord diameter after dissection were measured on the day of testing. The notochord diameter at the midpoint of each section was used during data processing. All other measurements were taken from photos in ImageJ2 (v.1.42q)[65].

Stem and early tetrapods. Measurements of *T. roseae* were taken using Blender[66] from a computed tomography reconstruction of the axial column of NUFV 108 by T.A.S. Measurements of *A. gunnari*, *G. burkemorani* and *T. insignis* were taken using Fiji[67] from two-dimensional reconstructions modified by B.K.A.O. from their source publications. Measurements of *W. deltae* were taken using Fiji[67] from two-dimensional reconstructions by B.K.A.O. based on direct observations (see Supplementary Fig. 7 caption and Supplementary Table 12 for references).

Data processing

Raw data were processed in R[68] and Rstudio[69] using the CrshR repository[70]. The CrshR functions are used to analyse each bending or torsion cycle. For bending, the functions produce the maximum bending load (N), maximum bending displacement (mm), maximum bending angle (degrees) and work done to achieve maximum displacement (Nm). For torsion, the functions produce the maximum torque (Nm) and the angle at maximum torque (degrees). These data were further processed and plotted in R using functions in the Korneisel_TetNecks_2026 repository[71] and the ggplot2, ggthemes, readr, dplyr and RColorBrewer packages[72–78]. Equations were published previously[79]; any modifications are indicated.

For bending trials, we first calculated the flexural rigidity (EI, Nm^2) using:

$$EI = \frac{FL^3}{48d} \tag{1}$$

where F is the maximum force (N), L is the three-point bending rig span (m) and d is the maximum displacement (m). We next used the following known equations for the second moment of area (I) to calculate Young's modulus (E). For the notochord, we used:

$$I_{\text{circle}} = \frac{\pi r^4}{4} \tag{2}$$

where r is the radius (m). For the vertebral column bent laterally, we used:

$$I_{\text{triLat}} = \frac{hb^3}{48} \tag{3}$$

and for the vertebral column bent dorsoventrally, we used:

$$I_{\text{triDV}} = \frac{h^3 b}{36} \tag{4}$$

where h is the height of the estimated vertebral triangle (m) and b is the base of the estimated vertebral triangle (m).

For torsion trials, we first calculated torsional rigidity (GJ, Nm^2 per radian) using:

$$GJ = \frac{TL}{\theta} \quad (5)$$

where T is the maximum torque (Nm), L is the gauge length (m) and θ is the angle at maximum torque (degrees). We next used the following known equations for the polar moment of area or torsional constant (J) to calculate the modulus of rigidity (G). For the notochord, we used:

$$J_{\text{circle}} = \frac{\pi D^4}{32} \quad (6)$$

where D is the diameter of the notochord (m). For the vertebral column, we used:

$$J_{\text{tri}} = \frac{hb}{144}(4b^2 + 3h^2). \quad (7)$$

The Young's modulus was calculated from the three-point bending data for each matching position or section between specimens under both dissection conditions, and the torsion constant was calculated from the torsion data for each section and under both dissection conditions, using the CrshR package in R[68–70].

Modelling of extinct taxa

The Young's modulus and the torsion constant for the axial column were determined from the measurements taken from the anterior-most axial column of *A. fulvescens* (Supplementary Table 1, bending position 1 (bending) and section number 1 (rotation)). The anterior position for whole-column bending and the first section for all other tests were posterior to the midline skull and fused occipital vertebrae but overlapped with the opercula in life, making them most comparable to the area of interest in stem tetrapods. The material values were then used to calculate lateral flexion, extension and rotation, along with I and J values obtained from the measurements of the neck region of each taxon (Extended Data Table 4 and Extended Data Fig. 2). These bending calculations revealed the force and the torsion calculations the torque needed to produce the deflections in the anterior axial column.

Lateral flexion estimation. For extinct taxa, the second moment of area for the anterior axial column was calculated using equation (3), and for the notochord using equation (2), on the basis of the measurements shown in Extended Data Table 4.

We used equation (8), which gives the deflection of a beam under cantilevered bending solved for force, to calculate the force required to achieve a specific lateral deflection. Data were collected using three-point bending rather than cantilevered bending. This is because the three-point set-up enables the paired supports to be placed closely, so that the soft tested material can start in a neutral position, rather than a bent one because of the force of gravity. Cantilevered bending, however, is a good approximation for the bowstring model of axial bending and was therefore used to model the estimated lateral flexion and extension.

$$F = \frac{\delta 3EI}{L^3} \quad (8)$$

In equation (8), δ is deflection, E is the calculated Young's modulus for position 1 (whole-column bending) or section 1 (all other measurements) of *A. fulvescens*, I is the second moment of area of the relevant axial-column section of the taxon of interest and L is the length of the cervical region or its equivalent.

For each of these equations, deflection was treated as the opposite end of a right triangle with the adjacent side length of L to determine the angle of deflection (equation (9)) using the ATAN function in Excel. This deflection was obtained in radians and converted to degrees using equation (10).

$$\tan^{-1}\left(\frac{\delta}{L}\right) \quad (9)$$

$$\delta_{\text{deg}} = \frac{\delta_{rad} \times 180}{\pi} \quad (10)$$

Striated muscle in vertebrates is known to generate pressures of 200–300 kPa (kilonewtons per square meter of muscle in cross-section)[79]. Using this known range, we calculated the muscle cross-sectional area required to achieve these forces. These muscle areas were capped for each taxon at half the area of an oval fitted around the posterior skull. This was chosen to provide the absolute maximum muscle area available to perform lateral flexion (area on one side) and extension (dorsal area of both sides combined; Supplementary Fig. 3). The angle of deflection produced by the maximum force from the corresponding muscle area in each species represents the estimated maximum range of motion for the animal.

Extension estimation. The second moment of area for the anterior axial column was calculated using equation (4). All other steps followed the same process as that for lateral flexion.

Rotation estimation. The polar moments of area for torsion on the column were calculated using equation (6) and for the notochord using equation (7). G was averaged from the sturgeon vertebral column, as it did not change significantly with position along the column. J was calculated from measurements of extinct taxa. We calculated torque (T) at small angles (5–10°) using equation (11), which is equation (5) solved for T:

$$T = \frac{GJ\theta}{L}. \quad (11)$$

For rotation, we started with small angles and found that the column required very high torques to achieve any rotation (Extended Data Table 1).

Validation

The method for estimating range of motion was validated by applying it to lungfish, an extant taxon, described in a previous study[80], in which elevation of the cranium was measured in vivo at a maximum of about 5° during feeding strikes over an axial column length of 5 cm. We measured the axial column and body cross-sectional area in computed tomography scans of the original specimens using Materialise Mimics (v.26.0). Our estimate of the maximum extension along this axial column length was 5.25° or 8.75°, depending on the proportions of each individual.

Reporting summary

Further information on research design is available in the Nature Portfolio Reporting Summary linked to this article.

Data availability

The data necessary to replicate our results are available at GitHub[71] (https://github.com/CDonatelli/Korneisel_TetNecks_2026) or at Figshare[81] (https://figshare.com/articles/dataset/Korneisel_TetNecks_2026/33552199?file=68415544). Materials not available in this paper, its Supplementary Information or the repository are available from the corresponding author. Source data are provided with this paper.

Code availability

The codes used to analyse universal testing machine output data are available at GitHub[70] (https://github.com/CDonatelli/CrshR).

Additional codes specific to the analysis of this method, as well as modifications to the base CrshR code, are available at GitHub[71] (https://github.com/CDonatelli/Korneisel_TetNecks_2026) or at Figshare[81] (https://figshare.com/articles/dataset/Korneisel_TetNecks_2026/33552199?file=68415544).

65. Rueden, C. T. et al. ImageJ2: ImageJ for the next generation of scientific image data. *BMC Bioinform.* **18**, 529 https://doi.org/10.1186/s12859-017-1934-z (2017).
66. Blender: a 3D modelling and rendering package v.4.0 http://www.blender.org (Stichting Blender Foundation, 2018).
67. Schindelin, J. et al. Fiji: an open-source platform for biological-image analysis. v1.54p. *Nat. Methods* **9**, 676–682 (2012).
68. R: a language and environment for statistical computing v.4.3.3 https://www.R-project.org (R Foundation for Statistical Computing, 2020).
69. RStudio: integrated development for R v.2023.12.1 http://www.rstudio.com (RStudio, 2019).
70. Donatelli, C. M. CrshR. *GitHub* https://github.com/CDonatelli/CrshR (2021).
71. Donatelli, C. M. Korneisel_TetNecks_2026. *GitHub* https://github.com/CDonatelli/Korneisel_TetNecks_2026 (2026).
72. Wickham, H. ggplot2: elegant graphics for data analysis. R v.4.0.1 https://ggplot2.tidyverse.org (2016).
73. Arnold, J. ggthemes: extra themes, scales and geoms for 'ggplot2'. R v.5.1.0.9000 https://github.com/jrnold/ggthemes (2025).
74. Wickham, H., Hester, J. & Bryan, J. readr: read rectangular text data. R v.2.1.5 https://readr.tidyverse.org (2024).
75. Wickham, H., François, R., Henry, L., Müller, K. & Vaughan, D. dplyr: a grammar of data manipulation. R v.1.1.4 https://dplyr.tidyverse.org (2025).
76. Neuwirth, E. RColorBrewer: ColorBrewer Palettes. R v.1.1-3 https://CRAN.R-project.org/package=RColorBrewer (2022).
77. Hibbeler, R. C. *Mechanics of Materials* 8th edn (Pearson Prentice Hall, 2010).
78. Wickham, H., Hester, J. & Bryan, J. readr: read rectangular text data. *GitHub* https://github.com/tidyverse/readr (2024).
79. Rospars, J.-P. & Meyer-Vernet, N. Force per cross-sectional area from molecules to muscles: a general property of biological motors. *R. Soc. Open Sci.* **3**, 160313 (2016).
80. Gartner, S. M. et al. Suction feeding of West African lungfish (*Protopterus annectens*): an XROMM analysis of jaw mechanics, cranial kinesis, and hyoid mobility. *Biol. Open* **11**, bio059447 (2022).
81. Donatelli C. M. Korneisel_TetNecks26. *figshare* https://doi.org/10.6084/m9.figshare.33552199 (2026).

Acknowledgements The sturgeon specimens used in this study were collected from the traditional territory of the Rainy River First Nations by members of that nation, and we are grateful for their stewardship of the waters that made sourcing these fish possible. We thank M. Chiasson, M. Wilkie, H. Flavio and the staff at the Ontario Aquaculture Research Center for raising and providing the specimens used in this study; Fabienne and Michel at Péché Fumé for providing specimens used to design the methods; colleagues in the Maddin lab for their help with this project; and S. Gartner for making her lungfish data available to us.

Author contributions D.E.K. and T.M. conceived the study, and D.E.K., E.M.S., C.M.D. and H.C.M. designed the study with early clamp designs provided by M.M. C.M.D. and L.H. designed the machine programs. C.M.D. coded the functions used for data analysis, performed calculations on sturgeon data and prepared tables and graphs for materials data. D.E.K., L.H. and A.L.T. performed the testing. T.A.S., B.K.A.O. and D.E.K collected and prepared the data on extinct taxa. D.E.K. performed the measurements and calculations for extinct taxa. D.E.K. wrote the manuscript and prepared Figs. 1 and 2 with considerable input for the methods from C.M.D. and general input from E.M.S., T.M. and H.C.M. D.E.K. wrote the Supplementary Information, and D.E.K. and C.M.D. prepared Extended Data Figs. 3–5.

Funding D.E.K. received funding for this research from The Steven Cohen Award for Student Research presented by the Society of Vertebrate Paleontology. H.C.M. received support for this research from the Natural Sciences and Engineering Research Council (RGPIN-06442). Open access funding provided by Uppsala University.

Competing interests The authors declare no competing interests.

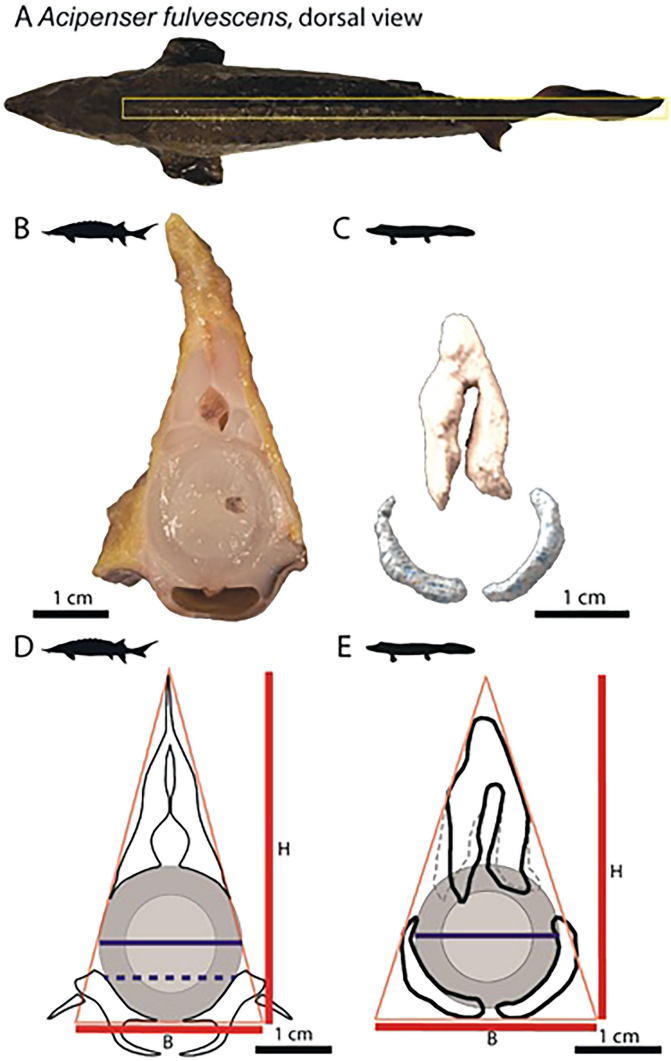
Additional information

Supplementary information The online version contains supplementary material available at https://doi.org/10.1038/s41586-026-11158-3.

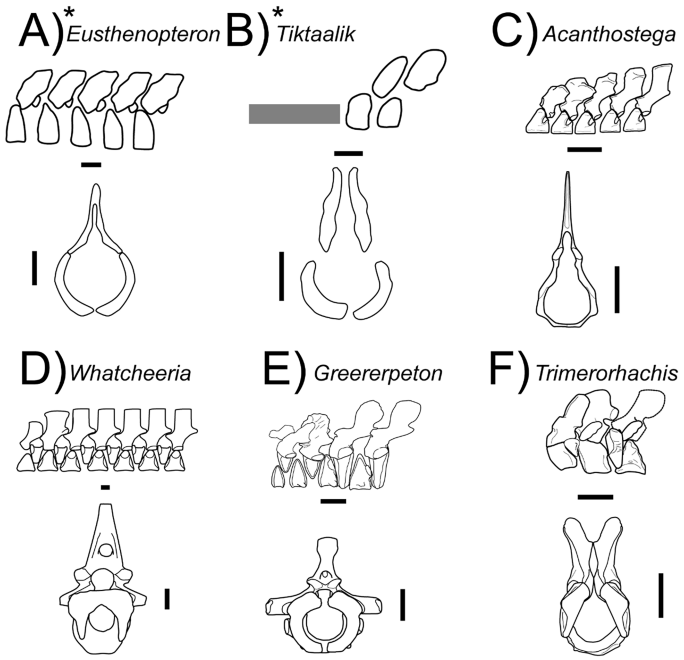
Correspondence and requests for materials should be addressed to Dana E. Korneisel.

Peer review information *Nature* thanks Kenneth Angielczyk, Tatsuya Hirasawa and the other, anonymous, reviewer(s) for their contribution to the peer review of this work. Peer reviewer reports are available.

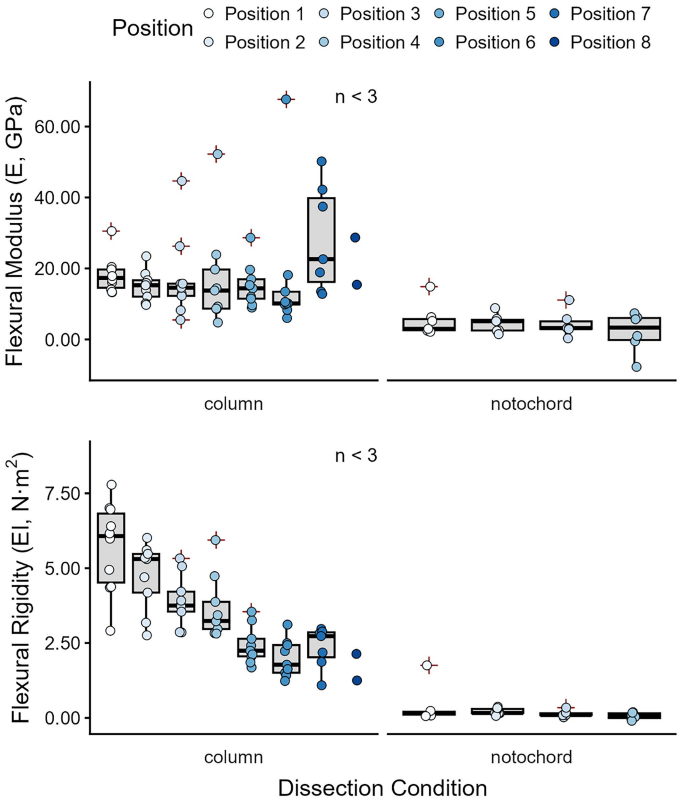
Reprints and permissions information is available at http://www.nature.com/reprints.



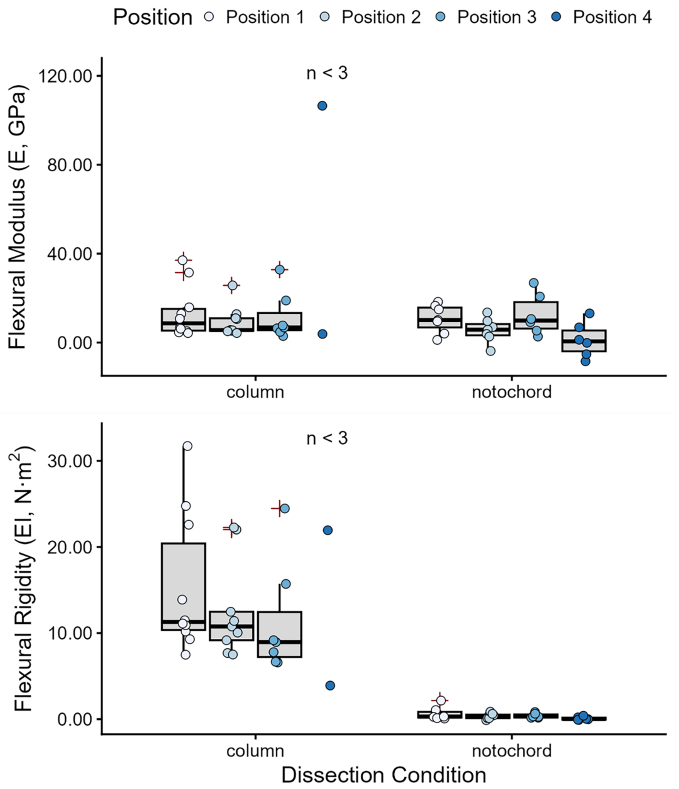
Extended Data Fig. 1 | Measurements for calculation of second moment of area and polar moment of area in sturgeon. *Acipenser fulvescens* (A, B, D), and stem tetrapods (C, E), represented here by an exemplar, *Tiktaalik roseae*. **A**. *A. fulvescens* individual in dorsal view with area dissected for testing marked in yellow. **B**. *A. fulvescens* anterior axial column in cross-sectional view. **C**. Surface rendering of the anterior-most well-preserved vertebra of *T. roseae* photographed in cross-sectional view. **D**. Line drawing of idealized sturgeon vertebra in cross-sectional view with measurements marked. **E**. Line drawing of *T. roseae* vertebra 4 in cross sectional view with measurements marked. An approximated retro-deformation of the neural arch pedicles is indicated by a grey dashed line. Blue lines indicate notochord diameter (solid) and intercentral span (dashed in sturgeon where intercentral span is only 96% of notochord diameter). Red lines indicate column measurements, B = base, H = height. Image in **c** reproduced from ref. 41, PNAS, under a creative Commons licence CC BY-NC-ND 4.0.



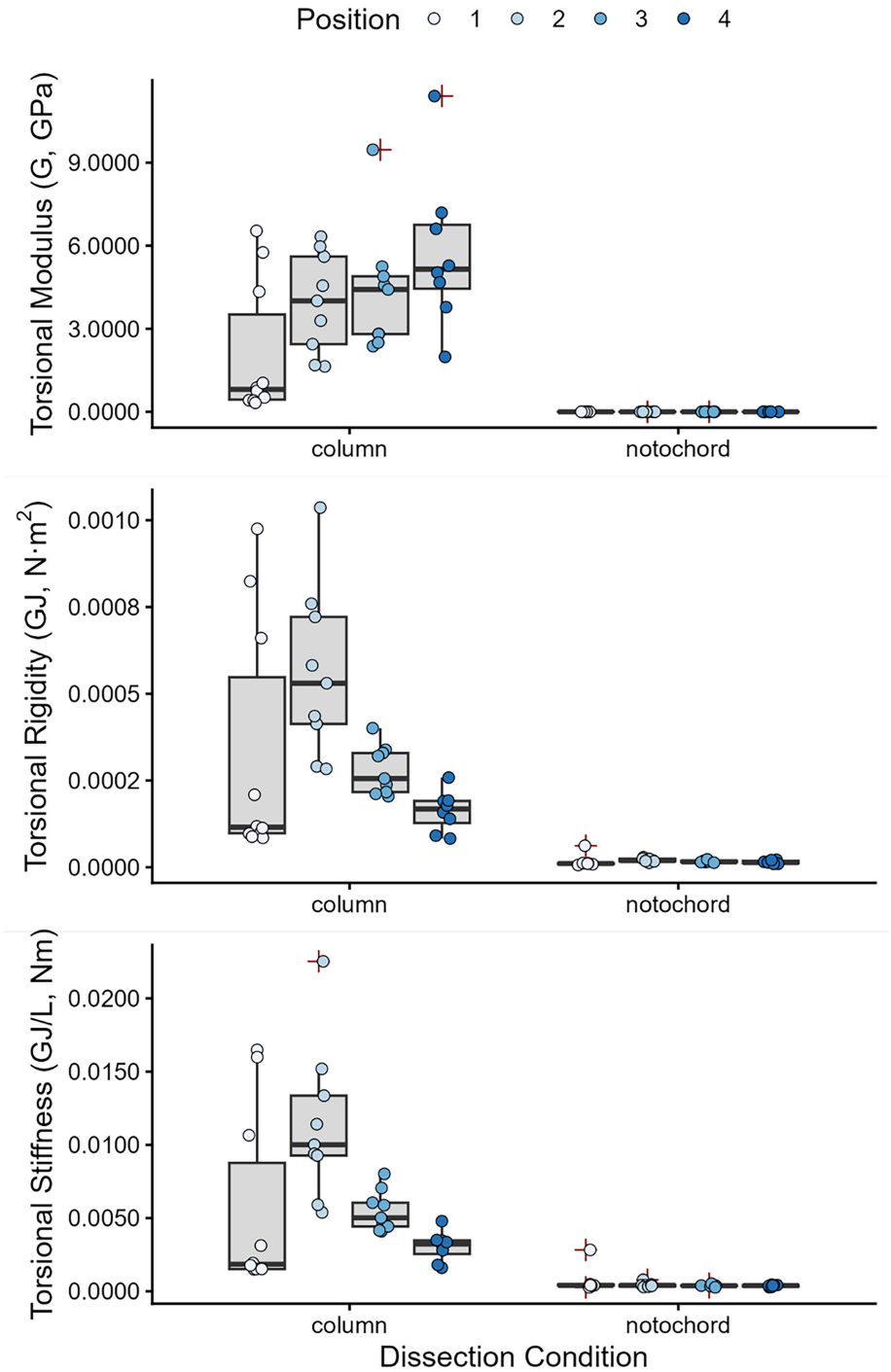
Extended Data Fig. 2 | Vertebral reconstructions for extinct taxa considered for this study. Taxa with a highly restricted notochordal canal were deemed too anatomically dissimilar from the analogue for mobility estimation. A. *Eusthenopteron foordi*: from Andrews and Westoll (1970), input from Hitchcock, 1995 also considered in this study. B. *Tiktaalik roseae*: C. *Acanthostega gunnari*: modified from Coates (1996), vertebra in anterior view is equivalent to the posteriormost cervical. D *Whatcheeria deltae*: modified from Otoo et al. (2021) by removal of the first centrum component from the original reconstruction following Korneisel et al. (2025)'s observation that this appears to have been a misplaced pleurocentrum, vertebra in anterior view is a posterior cervical reconstructed from isolated vertebral components. E. *Greererpeton burkemorani*: modified from Godfrey (1989a), vertebra in anterior view is V5. F. *Trimerorhachis insignis*: based on Case (1911), 1935, Shiskin (2000), and Pawley (2000), vertebra in anterior view is reconstructed from isolated centra and posterior trunk neural arches. *measurements in this study were not taken from this reconstruction. *Eusthenopteron* included supraneurals per Hitchcock (1995) and *Tiktaalik* measurements were taken directly from CT rendering. All scale bars 1 mm.



Extended Data Fig. 3 | Lateral bending results from 3-point bending trials of the lake sturgeon, *Acipenser fulvescens*. Flexural modulus is the same as Young's modulus. Colour of the jittered point represents position along the body. The solid line within the boxplot represents the median and the upper and lower limit of the box represents the first and third quartiles (25th and 75th percentiles). The distance between first and third quartiles is defined as the interquartile range (IQR). Whiskers extend to the furthest value that is 1.5x IQR. Points marked with a red cross indicate points outside of the IQR. No median or quartiles are presented for column lateral bending at position 8, as n = 2. Remaining sample sizes are as follows: Column position 1, n = 10; Column positions 2-6, n = 9; Column position 7, n = 8; Notochord position 1, n = 9; Notochord positions 2 & 3, n = 7; Notochord position 4, n = 6.



Extended Data Fig. 4 | Dorsoventral bending results from 3-point bending trials of the lake sturgeon, *Acipenser fulvescens*. Flexural modulus is the same as Young's modulus. Colour of the jittered point represents position along the body. The solid line within the boxplot represents the median and the upper and lower limit of the box represents the first and third quartiles (25th and 75th percentiles). The distance between first and third quartiles is defined as the interquartile range (IQR). Whiskers extend to the furthest value that is 1.5x IQR. Points marked with a red cross indicate points outside of the IQR. No median or quartiles are presented for column dorsoventral bending at position 4, as n = 2. Remaining sample sizes are as follows: Column position 1, n = 10; Column position 2, n = 9; Column position 3, n = 6; Notochord position 1, n = 9; Notochord position 2 & 3, n = 7; Notochord position 4, n = 6.



Extended Data Fig. 5 | Torsion testing results for the lake sturgeon, *Acipenserfulvescens*. Colour of the jittered point represents position along the body. The solid line within the boxplot represents the median and the upper and lower limit of the box represents the first and third quartiles (25th and 75th percentiles). The distance between first and third quartiles is defined as the interquartile range (IQR). Whiskers extend to the furthest value that is 1.5x IQR. Points marked with a red cross indicate points outside of the IQR. Column position 5 is excluded due to n = 1. Remaining sample sizes are as follows: Column positions 1-3, n = 9; Column position 4, n = 8; Notochord position 1, n = 9; Notochord position 2 & 3, n = 7; Notochord position 4, n = 6.

Extended Data Table 1 | Torque necessary for 5 degrees of head rotation in extinct taxa

Whole column

Taxon	Torque (Nm)	Neck length (cm)	Neck length (# of vertebrae)
Eusthenopteron foordi	314	3.69*	5*
Tiktaalik roseae	200	4.73	4
Acanthostega gunnari	485	3.57	5
Greererpeton burkemorani	456	4.44	4
Whatcheeria deltae	746	19.54	7
Trimerorhachis insignis	319	2.81	3

Notochord

Taxon	Torque (Nm)	Neck length (cm)	Notochord diameter (cm)
Eusthenopteron foordi	0.00185	3.69*	1.34
Tiktaalik roseae	0.00281	4.73	1.59
Acanthostega gunnari	0.00273	3.57	1.47
Greererpeton burkemorani	0.000653	4.44	1.08
Whatcheeria deltae	0.000176	19.54	1.13
Trimerorhachis insignis	0.000537	2.81	0.92

High torques would be necessary to twist the anterior axial column for even small head rotations, but the notochord alone is much less resistant to torsion. **E. foordi* does not have a cervical region. The first 5 vertebrae are anatomically distinct[30], so their length was used here, but they are overlapped by the opercular bones covering the gills.

Extended Data Table 2 | Maximum lateral flexion and extension estimates (degrees) for extinct taxa as limited by the axial column

Taxon	Lateral (˚)	Dorsal (˚)	Neck length (cm)	Neck length (# of vertebrae)
Eusthenopteron foordi	8.5	3	3.69*	5*
Tiktaalik roseae	5.5	2.25	4.73	4
Acanthostega gunnari	2.75	0.6	3.57	5
Greererpeton burkemorani	2	1.4	4.44	4
Whatcheeria deltae	32	12	19.54	7
Trimerorhachis insignis	1	0.25	2.81	3

Estimates, also imaged in Fig. 2, with original sources referenced for neck length corresponding to Extended Data Fig. 2, as follows: *Eusthenopteron*[30], *Tiktaalik*[41], *Acanthostega*[2], *Greererpeton*[43], *Whatcheeria*[42], *Trimerorhachis*[44–47]. *First five vertebrae and length across their centra.

Extended Data Table 3 | Specimens used for Materials Testing

Specimen Number	Skull cube to tail length (cms)	Number of lateral bending positions	Number of dorsoventral bending positions	Number of Sections (# notochord sections if different)	Notes
2401-01	37.7	6	4	4(1)	Only anteriormost notochord dissected due to time constraints
2401-02	37.5	1	1	5(1)	Right side notochord damaged during dissection, only 1 testable location
2401-03	38.6	7	2	0	No notochord sections dissected due to time constraints, small rotation was observed in dorsal end of fish during dorso-ventral bending
2401-04	39.7	8	3	3	Notochord section 3 badly damaged during dissection, not tested
2401-05	43.2	7	3	4	
2401-06	36.9	7	3	4	Minor anterior damage and moderate posterior damage to notochord section 4 during dissection, these portions were outside of testing area for bending and trimmed before torsion testing
2401-07	40.4	7	2	4	
2401-08	40.2	8	3	4	
2401-09	39.9	7	4	4	
2401-10	41.5	7	2	4	
1126-01	not tested, used for practice dissection and clamp fitting, depicted in Figure S4				

Specimen Number	Nose to tail length (cms)	Used for	Notes
0923-01	104	Practice dissections, clamp design, and protocol troubleshooting; 0923-01 depicted in Extended Data Figure 4	Notochord exposed during filleting by fishers
0923-02	101		

Acipenser fulvescens specimens used for design and implementation of materials tests.

Extended Data Table 4 | Area of interest measurements from extinct taxa

Taxon	Source(s)	Base (cm)	Height (cm)	Length (cm, across centra)	Intercentral Span (cm)
Eusthenopteron foordi	Andrews & Westoll, 1970; Hitchcock, 1995	2.55	4.34	3.69	1.40
Tiktaalik roseae	Stewart et al., 2024 + TAS	2.55	3.97	4.73	1.65
Acanthostega gunnari	Coates, 1996	2.43	5.26	3.57	1.53
Greererpeton burkemorani	Godfrey, 1989a	3.44	4.4	4.44	1.13
Whatcheeria deltae	Otoo, et al. 2021 + BKAO	4.87	8.09	19.54	1.18
Trimerorhachis insignis	Case, 1911; 1935; Shiskin, 2000; Pawley, 2000	1.56	3.11	2.81	0.96

Sources and linear measurements necessary to perform deflection calculations to estimate mobility.

nature portfolio

Corresponding author(s): Dana E. Korneisel

Last updated by author(s): Aug 28, 2026

Reporting Summary

Nature Portfolio wishes to improve the reproducibility of the work that we publish. This form provides structure for consistency and transparency in reporting. For further information on Nature Portfolio policies, see our Editorial Policies and the Editorial Policy Checklist.

Statistics

For all statistical analyses, confirm that the following items are present in the figure legend, table legend, main text, or Methods section.

n/a	Confirmed
☐	☒ The exact sample size (*n*) for each experimental group/condition, given as a discrete number and unit of measurement
☐	☒ A statement on whether measurements were taken from distinct samples or whether the same sample was measured repeatedly
☒	☐ The statistical test(s) used AND whether they are one- or two-sided *Only common tests should be described solely by name; describe more complex techniques in the Methods section.*
☒	☐ A description of all covariates tested
☒	☐ A description of any assumptions or corrections, such as tests of normality and adjustment for multiple comparisons
☐	☒ A full description of the statistical parameters including central tendency (e.g. means) or other basic estimates (e.g. regression coefficient) AND variation (e.g. standard deviation) or associated estimates of uncertainty (e.g. confidence intervals)
☒	☐ For null hypothesis testing, the test statistic (e.g. *F*, *t*, *r*) with confidence intervals, effect sizes, degrees of freedom and *P* value noted *Give P values as exact values whenever suitable.*
☒	☐ For Bayesian analysis, information on the choice of priors and Markov chain Monte Carlo settings
☒	☐ For hierarchical and complex designs, identification of the appropriate level for tests and full reporting of outcomes
☒	☐ Estimates of effect sizes (e.g. Cohen's *d*, Pearson's *r*), indicating how they were calculated

Our web collection on statistics for biologists contains articles on many of the points above.

Software and code

Policy information about availability of computer code

Data collection	Programs for data collection on the Universal Testing Machine were written by CMD with modifications by LH. The parameters are listed in the extended data methods section. Blender (version 4.0) was used for linear measurements on 3D data. Fiji (version #####) was used for linear measurements on 2D data from fossil material and sturgeon. Fiji (version v1.54p) was used during revision to check measurements.
Data analysis	Code was written by CMD in R (version 4.3.3) used with RStudio (version 2023.12.1) using code written for the CrushR package with some functions specialized for use in this study (the base package, previously published is available at github: https://github.com/CDonatelli/CrshR, all specialized code for this study is also present in the following repository). Data and additional code for their analysis as well as the specialized code using CrushR are available in the github repository Korneisel_TetNecks_2026 which can be accessed through https://github.com/CDonatelli/Korneisel_TetNecks_2026 or through Figshare with the identifier "10.6084/m9.figshare.33552199" or using the link: https://figshare.com/articles/dataset/Korneisel_TetNecks_2026/33552199?file=68415544. The R packages ggplot2 (version 4.0.1), ggthemes (version 5.1.0.9000), readr (version 2.1.5), dplyr (version 1.1.4), and RColorBrewer (version 1.1-3) are used in data analysis and plotting.

For manuscripts utilizing custom algorithms or software that are central to the research but not yet described in published literature, software must be made available to editors and reviewers. We strongly encourage code deposition in a community repository (e.g. GitHub). See the Nature Portfolio guidelines for submitting code & software for further information.

Data

Policy information about availability of data

All manuscripts must include a data availability statement. This statement should provide the following information, where applicable:

- Accession codes, unique identifiers, or web links for publicly available datasets
- A description of any restrictions on data availability
- For clinical datasets or third party data, please ensure that the statement adheres to our policy

The original data for this study are available within the GitHub repository https://github.com/CDonatelli/Korneisel_TetNecks_2026, owned and managed by CMD, presented in excel spreadsheets.

Research involving human participants, their data, or biological material

Policy information about studies with human participants or human data. See also policy information about sex, gender (identity/presentation), and sexual orientation and race, ethnicity and racism.

Reporting on sex and gender	No human participants or material were used in this study.
Reporting on race, ethnicity, or other socially relevant groupings	No human participants or material were used in this study.
Population characteristics	No human participants or material were used in this study.
Recruitment	No human participants or material were used in this study.
Ethics oversight	No human participants or material were used in this study.

Note that full information on the approval of the study protocol must also be provided in the manuscript.

Field-specific reporting

Please select the one below that is the best fit for your research. If you are not sure, read the appropriate sections before making your selection.

☒ Life sciences ☐ Behavioural & social sciences ☐ Ecological, evolutionary & environmental sciences

For a reference copy of the document with all sections, see nature.com/documents/nr-reporting-summary-flat.pdf

Life sciences study design

All studies must disclose on these points even when the disclosure is negative.

Sample size	Ten Acipenser fulvescens specimens were used in this study as each could be used for multiple measurements along the length of the body as well as for three different types of movement. It is imperative for biomechanical study that the specimens be tested as freshly as possible and in as similar a condition as possible. The ultimate sample size was limited for this reason and because dissection of each sample before and during testing was very time consuming, limiting each testing day to 3-4 specimens.
Data exclusions	Data were excluded when there were issues during the collection cycle (see extended data methods section) such as the specimen falling over during testing. Exclusion criteria were pre-established in the experimental design and data that would need to be excluded were identified during testing.
Replication	Testing took place on three separate days but each material test was performed once at each location except in cases where the specimen fell out of alignment (in these cases, the test was attempted a second time). These tests were repeated at the same locations on multiple specimens (see extended data tables 1-3 for process and numbers). All details of specimen preparation for testing including detailed dissection images are provided in the extended data to make the precise testing conditions repeatable by any interested party.
Randomization	This study did not allocate specimens into different experimental groups as it was focused on collecting non-experimental biomechanical data.
Blinding	This study did not involved experimental groups, so no blinding protocol was used.

Reporting for specific materials, systems and methods

We require information from authors about some types of materials, experimental systems and methods used in many studies. Here, indicate whether each material, system or method listed is relevant to your study. If you are not sure if a list item applies to your research, read the appropriate section before selecting a response.

Materials & experimental systems

n/a	Involved in the study
☒	☐ Antibodies
☒	☐ Eukaryotic cell lines
☐	☒ Palaeontology and archaeology
☐	☒ Animals and other organisms
☒	☐ Clinical data
☒	☐ Dual use research of concern
☒	☐ Plants

Methods

n/a	Involved in the study
☒	☐ ChIP-seq
☒	☐ Flow cytometry
☒	☐ MRI-based neuroimaging

Palaeontology and Archaeology

Specimen provenance	All specimens utilized in this study were collected and described by previous researchers. Measurements were taken from published data and the source publications are listed in the references sections as well as in figure captions where relevant.
Specimen deposition	All specimens utilized in this study were described by previous researchers and are in collections readily available to researchers. Their accession information can be found in the relevant referenced articles.
Dating methods	No new dates are provided in this study.

☐ Tick this box to confirm that the raw and calibrated dates are available in the paper or in Supplementary Information.

Ethics oversight	No ethical approval or guidance was necessary for this study as the palaeontological specimens used herein did not require it as all material is already present in the literature.

Note that full information on the approval of the study protocol must also be provided in the manuscript.

Animals and other research organisms

Policy information about studies involving animals; ARRIVE guidelines recommended for reporting animal research, and Sex and Gender in Research

Laboratory animals	This study did not include any laboratory animals.
Wild animals	The Acipenser fulvescens individuals used in this study were sourced after euthanasia at approximately 1 year of age. They were originally obtained from the wild as fertilized eggs by members of the Rainy Rivers First Nation in collaboration with the Ontario Aquaculture Research Center and raised at the research center before being moved by ground transport to Wilfrid Laurier University where they were housed until reaching approximately one year of age. After experimentation there, the remains of euthanized fish were provided to us.
Reporting on sex	Sex was not considered in this study design and the fish were not sexed during testing. There is no reason to believe that sex has any effect on the axial column biomechanics of Acipenser fulvescens.
Field-collected samples	This study did not involve any newly collected animals from the field. See 'wild animals' section for more information on specimen provenance.
Ethics oversight	Neither ethical guidance nor approval were necessary for this study as the study organisms were all sourced dead. The fish used in this study that were not sourced from waste from commercial fishing were housed and cared for in accordance with the Canadian Council on Animal Care and Wilfrid Laurier University's Animal Care Committee approved animal use protocol (AUP #22003).

Note that full information on the approval of the study protocol must also be provided in the manuscript.

Plants

Seed stocks	No plants were used in this study.
Novel plant genotypes	No plants were used in this study.
Authentication	No plants were used in this study.